Nonlinear Modeling and Control of Polyvinyl Chloride (PVC) Gel Actuators

Mohammed Al-Rubaiai, Xinda Qi, Zachary Frank, Ryohei Tsuruta, Umesh Gandhi, Kwang J. Kim, and Xiaobo Tan, *Fellow, IEEE*

***Abstract*—Polyvinyl chloride (PVC) gels represent a novel type of electroactive polymer actuators with a number of appealing characteristics, including low cost, high compliance, large strain, medium-to-high stress output, fast response, and thermal stability. Despite their vast potential in a variety of applications, modeling and control of nonlinear dynamics of PVC actuators has received little attention. In this article, we first present a data-driven approach to modeling nonlinear dynamics of PVC gel actuators. A Hammerstein model, consisting of a nonlinear module cascaded with linear dynamics, is proposed to capture the pronounced dependence of the voltage input–displacement output frequency response on the input amplitude and bias. A control scheme is then designed based on the model, where an inverse compensator for the nonlinear element is combined with a PID feedback controller. A disturbance observer is further introduced for the estimation and rejection of the influences from imperfect inverse compensation and model uncertainties. Experimental results are presented to support the efficacy of the proposed modeling and control approach. In particular, for a number of reference trajectories, the proposed control scheme results in over 80% reduction of tracking error in comparison with a well-tuned PID controller.**

***Index Terms*—Describing function, electroactive polymer, frequency response, Hammerstein model, inverse control, polyvinyl chloride (PVC) gel actuator.**

Manuscript received 20 January 2022; revised 26 March 2022 and 5 May 2022; accepted 8 May 2022. Date of publication 6 June 2022; date of current version 16 August 2022. Recommended by Technical Editor Y.-J. Pan and Senior Editor Xiang Chen. This work was supported in part by Toyota Motor North America and a Michigan State University Strategic Partnership under Grant 16-SPG-Full-3236. The work of Zachary Frank and Kwang J. Kim was supported in part by the U.S. National Science Foundation (NSF), Partnerships for International Research and Education (PIRE) Program, under Grant 1545857. *(Corresponding author: Mohammed Al-Rubaiai.)*

Mohammed Al-Rubaiai, Ryohei Tsuruta, and Umesh Gandhi are with the Toyota Motor North America, Ann Arbor, MI 48105 USA (e-mail: mohammed.alrubaiai@toyota.com; ryohei.tsuruta@toyota.com; umesh.gandhi@toyota.com).

Xinda Qi and Xiaobo Tan are with the Department of Electrical and Computer Engineering, Michigan State University, East Lansing, MI 48824 USA (e-mail: qixinda@msu.edu; xbtan@msu.edu).

Zachary Frank and Kwang J. Kim are with the Department of Mechanical Engineering, University of Nevada, Las Vegas, NV 89154 USA (e-mail: zachary.frank@unlv.edu; Kwang.Kim@unlv.edu).

Color versions of one or more figures in this article are available at https://doi.org/10.1109/TMECH.2022.3175445.

Digital Object Identifier 10.1109/TMECH.2022.3175445

I. Introduction

SMART materials-based soft actuators have been widely studied because of their compactness, flexibility, and potential in practical applications [1]–[3]. Polyvinyl chloride (PVC) gel actuators, as a type of electroactive polymers, exhibit attractive performance in output displacement, force generation, actuation speed, and deformation stability. For example, Li *et al.* [4] demonstrated a planar PVC gel actuator with strain of 21%, output stress of over 0.6 MPa (twice as much as that of the skeletal muscle), and response time of 90 ms, under a driving electric field around $2\ \mathrm{V}/\mu\mathrm{m}$. These properties make PVC gel actuators a promising option for artificial muscle applications [5]–[8], including, for example, optical lenses, wearable devices, haptic interfaces, vibrotactile actuators, and microgrippers [9]–[14].

Along with the development of actuator designs, the underlying actuation mechanism for PVC gels has been examined. PVC and plasticizer molecules move and rearrange under a strong electric field because of their polarity, inducing electrophoresis current and charge injection from the cathode [15]. It is shown that the creeping motion of the gel into an anode with a mesh structure is closely related to the formation of a layer that is plasticizer-rich in the PVC gel [8]. A recent study shows the integral role of the conductivity and dielectric properties in the function of PVC gel actuators [16]. Based on some of these observations, mathematical models have been developed, including a bending model with plasticizer-rich layer theory [17], a model with equivalent circuit analysis [18], a model for force and deformation of the actuator based on Hill's muscle model [19], and an electromechanical model to describe the PVC gel actuator incorporating ionic liquids [20]. Furthermore, a numerical model based on nonlinear elasticity and Maxwell stress tensor has been developed for FEM simulations of PVC gel actuators [21]. While these models are in general useful in predicting static output deformation and force, models describing nonlinear dynamic behavior for PVC gel actuators that are suitable for control, to the best of our knowledge, have not been reported in the literature. Such models will be important for advanced controller designs for these actuators in their practical applications. For the control of PVC gel actuators, a PD feedback controller is used in most existing studies, where nonlinear dynamics of such actuators have not been accounted for [7], [22].

We note that nonlinear effects in PVC gels arise due to several factors, such as nonlinear transport dynamics of charges and plasticizer molecules, and nonlinear elasticity of the PVC gel.

Proper accommodation of nonlinear dynamics in modeling and control of PVC gel actuators will enable the actuators to operate with accuracy within a large working range (both in terms of magnitude and frequency).

In this article, we present the first effort to characterize and model the nonlinear dynamic behavior of PVC gel actuators, where the frequency response from the voltage input to the displacement output shows significant dependence on the amplitude and bias of the voltage input. We consider a Hammerstein-type model for PVC gel actuators, consisting of a static nonlinearity followed by a dynamic module. The choice of this model structure is motivated by that PVC gel actuators, like many other smart material actuators (see, e.g., [23]), exhibit nonlinear but relative fast electrical (charge) dynamics with respect to their mechanical/structural dynamics. In addition, the charge dynamics drives the mechanical dynamics. In particular, the proposed model consists of a polynomial nonlinearity followed by linear dynamics. A systematic approach to the parameter identification is developed with the describing function machinery. While the classical describing function theory only captures the nonlinear dependence of the frequency response on the input amplitude, a key innovation of this work involves extending the method to incorporate the nonlinear effect of the input bias. The capability of the developed model to predict the dynamic response of the actuator with various inputs validates the model's effectiveness.

A trajectory-tracking controller is then developed based on the aforementioned nonlinear dynamic model, which combines an inverse compensator for the nonlinearity with a PID controller (termed "inverse/PID"). A disturbance observer (DOB) and compensator structure are further integrated with the inverse/PID scheme (termed "inverse/PID/DOB") to mitigate the influence of imperfect inversion, model uncertainties, and disturbances. Experimental results on tracking references of different frequencies (including multifrequency references) show the efficacy of the proposed control method. In particular, the averaging tracking error for the inverse/PID method is reduced by over 60% compared to a well-tuned PID controller; with the inverse/PID/DOB controller, the error reduction is further increased to over 80%.

Some preliminary results on the modeling of PVC gel actuators were reported at the 2021 MECC conference [24]. This article represents a significant enhancement over [24] in multiple ways. First, on the modeling side, while [24] only considered the nonlinearity with respect to the input amplitude, this work encompasses the nonlinear dependence of actuator dynamics on both input amplitude and input bias. Second, a major contribution of this article is the proposal of a nonlinear model-based control scheme, a subject our earlier work [24] did not touch at all. All experimental results in this article, including both modeling results and control results, are new.

The remainder of the article is organized as follows. The PVC gel membrane fabrication process is first presented in Section II. The modeling approach is discussed in Section III, followed by the controller design in Section IV. Section V presents the experimental results on model identification/validation and tracking control. Finally, Section VI concludes this article.

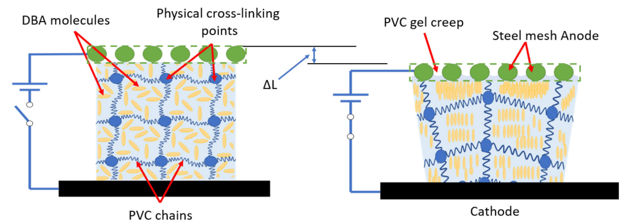

Fig. 1. Illustration of the PVC gel internal structure and the working mechanism of a contractile-type PVC gel actuator with a mesh anode. (a) Weakly linked PVC chains and randomly distributed plasticizer molecules in the absence of an electric field. (b) Polarization of PVC chains and plasticizers and migration of plasticizers toward the anode under an electric field, resulting in gel creeping into the mesh anode and bulk contraction along the thickness direction.

II. PVC Gel Fundamentals and Fabrication

The PVC gel contains PVC polymer chains that are loosely joined via physical crosslinking, with a plasticizer filling the interior space of the polymer chain matrix (Fig. 1). The exact actuation mechanism for PVC gels is still a subject of active research [6], where a few hypotheses have been examined. For example, Hashimoto [22] proposed that the electrostatic force between the gel and the anode, induced by charges injected from the cathode and migrating towards the anode, contributes to the actuation. The work by Chowdhury *et al.* [23] suggested that the polarization of the PVC chains and plasticizer molecules under an electric field, along with the migration of the plasticizers, generates the Maxwell stress that causes gel deformation and stretch along the anode surface. Xia and Hirai [15] argued that a thin solvent-rich (S-R) layer forms close to the anode and the resulting Maxwell stress between the S-R layer and the anode leads to the gel deformation. Regardless of the exact actuation mechanism, it has been widely observed that the gel shows asymmetric "anodophilic" deformation, a tendency of moving toward the anode. In particular, for a mesh anode, the PVC gel will creep into the holes in the mesh under an electric field. As a result, the actuator undergoes a bulk contraction in the thickness direction (see Fig. 1). Because of the elasticity of the gel, when the dc field is removed, the actuator quickly returns to its previous shape. Other types of actuation (such as bending) can be achieved using different arrangements of PVC gel and electrodes [7]. As shown in Table II in [7], reported response times for PVC gel actuators vary, but they are typically at the orders of 0.1–1 s, which is consistent with the results in our work, as seen later in Section V.

PVC gel membranes are commonly cast and they range in thickness from a few micrometers to several millimeters. In fabrication, PVC granules and DBA plasticizer (Sigma-Aldrich, St. Louis, MO, USA) are first mixed with the tetrahydrofuran (THF) solvent (Sigma-Aldrich, St. Louis, MO, USA). To fully dissolve the PVC and DBA in THF, the solution is agitated for 4 h at 50°C. To make a flat PVC gel membrane, one pours the totally dissolved solution into a glass Petri dish and leaves it at room temperature for 48 h, or until THF has evaporated. A fabricated sample, which is soft and transparent, can be seen in Fig. 2. The weight ratio of PVC to DBA can be changed to

Fig. 2. A photograph of a fabricated PVC gel membrane.

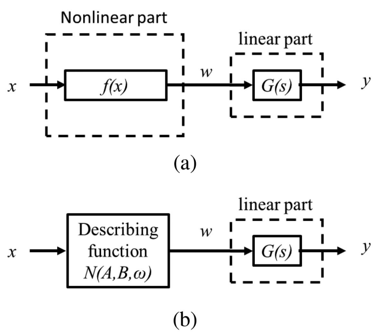

Fig. 3. (a) Proposed Hammerstein model structure for PVC gel actuator dynamics. (b) Use of the describing function of the nonlinear element for system identification.

modulate the material properties of the membranes, and a weight ratio of 1:6 (PVC to DBA) is used in this investigation.

III. Modeling Approach

The amplitude and bias of the voltage input affect the dynamic behavior of the PVC gel actuator (see the measured frequency responses in Fig. 7). In this article, we propose a Hammerstein model structure, which consists of a static nonlinearity $f(x)$ followed by a linear time-invariant (LTI) system, as shown in Fig. 3(a). As we elaborate shortly, the describing function method [Fig. 3(b)] will be used to facilitate the parameter identification for the nonlinearity based on measured frequency responses for the PVC actuator. The describing function approach is an enhanced form of the frequency response method that can be used to evaluate and forecast nonlinear behavior with reasonable accuracy [25]. In particular, for an LTI system, one can represent its behavior through the Bode plots (so-called "frequency response") that show the gain and phase-shift between the input and the output at different input frequencies, which are independent of the amplitude (or bias) of the applied input. However, for a nonlinear dynamic system, its "frequency response" depends on the operating regime of the system; namely, its behavior is only approximated by a linear system locally around some operating point. Such operating regimes can be characterized by the amplitude and/or the bias of the input. By collecting the input/output data under different input frequencies, amplitudes, and biases, we can extract the frequency response of the system in different operating regimes. The latter can then be used to identify the nonlinear function $f(x)$ and the transfer function $G(s)$ in the Hammerstein model structure, through the describing function machinery.

Typically, the describing function $N_0(A,\omega)$ of a nonlinear system is represented as

$$N_0(A,\omega) = \frac{Y}{A}\angle\phi \tag{1}$$

where A and ω represent the amplitude and the angular frequency of the sinusoidal input, respectively, Y denotes the amplitude of the fundamental harmonic component of the output, and ϕ denotes the phase shift of the fundamental harmonic component of the output with respect to the sinusoidal input. While typical describing functions only consider the dependence on the input amplitude A, in this work, we introduce a describing function that depends on both the amplitude A and the bias B, $N(A,B,\omega)$, to better capture the operating regimes of the PVC gel actuator. While there are many potential choices for the nonlinearity $f(x)$, in this work, we choose the class of polynomial functions given their simplicity and ability to describe the amplitude-dependent nonlinearity. We further narrow the choice to the group of odd polynomials to preserve the observed monotonicity of the actuation behavior—for a quasi-static input voltage, the displacement output of PVC gel actuator varies monotonically with the input. Such a property could be violated if even-powered terms were included in the polynomial. In particular, the considered nonlinearity takes the following form:

$$w = f(x) = \sum_{i=1}^{n} c_i x^{2i-1} \tag{2}$$

for some $n \geq 1$, where x is the input to the static nonlinearity, and c_i, $i = 1,\ldots,n$, are coefficients.

We first illustrate the computation of the describing function $N(A,B,\omega)$ with an example of $n = 2$, where

$$w = c_1 x + c_2 x^3. \tag{3}$$

Given an input $x(t) = B + A\sin(\omega t)$, we obtain from (3) the output $w(t) = c_1(B + A\sin(\omega t)) + c_2(B + A\sin(\omega t))^3$. Let the fundamental frequency component of $w(t)$ be denoted as $w_1(t)$, i.e.,

$$w_1(t) = a_1\cos(\omega t) + b_1\sin(\omega t) \tag{4}$$

where a_1 and b_1 are coefficients that can be readily evaluated based on $w(t)$, using the standard Fourier series expansion procedure [26]: $a_1 = 0$, and

$$b_1 = c_1 A + 3c_2\left(B^2 A + \frac{A^3}{4}\right). \tag{5}$$

Therefore, we have

$$w_1(t) = \left[c_1 A + 3c_2\left(B^2 A + \frac{A^3}{4}\right)\right]\sin(\omega t) \tag{6}$$

and the describing function as

$$N(A,B,\omega) = c_1 + 3c_2\left(B^2 + \frac{A^2}{4}\right). \tag{7}$$

Note that due to the polynomial nature of this nonlinearity, the describing function is real.

Since the LTI system $G(s)$ in Fig. 3 represents approximate, linear dynamics when the system operates in a localized regime, one can identify it based on the measured frequency response when the input amplitude is relatively small, at some given input bias. In this work, as discussed later in Section V-B, $G(s)$ is identified with the empirical frequency response data collected with input amplitude of 300 V (smallest among the amplitudes tested), and with input bias of 450 V (median among the biases tested). We now describe how to use $G(s)$, along with the describing function for the nonlinear element (parameterized with c_i, $i = 1, \ldots, n$), to identify c_i based on experimentally measured frequency responses at different input amplitudes and biases.

Let the frequency response of $G(s)$ be denoted as

$$G(j\omega) = M_L(\omega)\angle\psi(\omega) \tag{8}$$

where $M_L(\omega)$ and $\psi(\omega)$ represent the gain and phase shift, respectively, of $G(s)$ at the frequency ω. The overall gain for the Hammerstein system in Fig. 3 can be represented as

$$\begin{aligned} M_s(A, B, \omega) &= N(A, B, \omega)M_L(\omega) \\ &= \sum_{i=1}^{N} c_i h_i(A, B, \omega) \end{aligned} \tag{9}$$

where $h_i(A, B, \omega)$, $i = 1, \ldots, n$, represent the describing function terms associated with c_i. For example, when $n = 2$, from (7), $h_1 = M_L(\omega)$, $h_2 = 3(B^2 + \frac{A^2}{4})M_L(\omega)$.

Let us now assume that there are $N \geq n$ measurements of the overall system gain, $\{d_k(A_k, B_k, \omega_k)\}_{k=1}^{N}$, for different combinations of input frequencies ω_k, amplitudes A_k, and biases B_k. We would like to find the parameters $\{c_i\}_{i=1}^{n}$ by matching the measurements $\{d_k\}_{k=1}^{N}$ to the model predictions $\{M_s(A_k, B_k, \omega_k)\}_{k=1}^{N}$ via the least-squares optimization. To do this, we solve

$$\min_{C} \frac{1}{2} \parallel HC - d \parallel_2^2 \tag{10}$$

where $H = \begin{bmatrix} h_1(A_1, B_1, \omega_1) & \cdots & h_n(A_1, B_1, \omega_1) \\ h_1(A_2, B_2, \omega_2) & \cdots & h_n(A_2, B_2, \omega_2) \\ \cdots & & \cdots \\ h_1(A_N, B_N, \omega_N) & \cdots & h_n(A_N, B_N, \omega_N) \end{bmatrix}$,

$C = \begin{bmatrix} c_1 \\ c_2 \\ \cdots \\ c_n \end{bmatrix}$, and $\quad d = \begin{bmatrix} d_1(A_1, B_1, \omega_1) \\ d_2(A_2, B_2, \omega_2) \\ \cdots \\ d_N(A_N, B_N, \omega_N) \end{bmatrix}$.

The least-squares optimization problem in (10) can be solved using the Matlab command *lsqnonlin*. The found values of $\{c_i\}_{i=1}^{n}$ are then plugged into (2) to obtain the nonlinearity $f(x)$.

IV. Controller Design

Aside from the nonlinear dynamics, the estimation of disturbances and model uncertainties and the mitigation of their impacts are important to achieving good control performance for soft actuators. In this work, we propose the combination of inverse compensation, disturbance rejection, and feedback control to accommodate the system nonlinearity, inversion error, and unmodeled dynamics, as illustrated in Fig. 4.

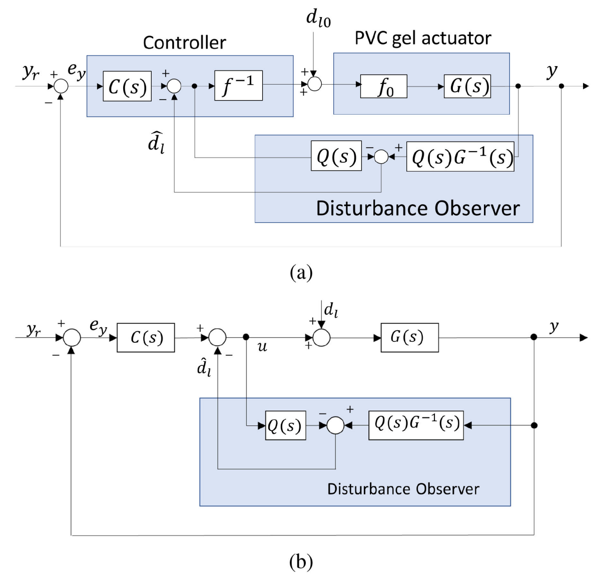

Fig. 4. (a) Diagram of the proposed inversion-based, disturbance-rejected, feedback control structure (inverse/PID/DOB). (b) Diagram of the closed-loop system upon the approximate cancelation of the nonlinearity by the inverse compensator. Note that d_{l0} in (a) represents the physical disturbance to the system, which is different from the effective disturbance d_l shown in (b), which represents the aggregated effect of physical disturbance, imperfect inversion, and unmodeled dynamics. The static nonlinearity f_0 in the plant model in (a) could be different from the identified nonlinearity f, and the resulting inversion error will contribute to the effective disturbance.

First, given the Hammerstein model structure as shown in Fig. 3(a), we propose placing an inverse of the nonlinearity f at the output end of the controller to (approximately) cancel the nonlinear effect, in which case one could design a linear controller $C(s)$ based on the remaining dynamics $G(s)$. Note that the identified static nonlinearity f (which is used to compute the inverse) will only be an approximation to the actual nonlinearity [denoted f_0 in Fig. 4(a)]. In this work, the command *finverse* in Matlab is used to compute the inverse of the static nonlinearity, f^{-1}, and $C(s)$ is chosen to be a PID controller due to its simplicity. We note that while the coefficients of $f(x)$ were identified with the frequency response data, the controller (including both $C(s)$ and f^{-1}) is able to handle reference trajectories of general forms (i.e., not restricted to sinusoidal waveforms).

Next, a disturbance observer is further used to estimate the "effective" disturbance d_l to the linear system $G(s)$, which accounts for imperfect inverse compensation, unmodeled dynamics, and disturbances. The estimated disturbance $\hat{d}_l$ is then subtracted from the output of $C(s)$ for disturbance rejection. We note that, with such an approach, the control scheme has some built-in robustness against modeling errors for both the static nonlinearity f and the transfer function $G(s)$. The design of the disturbance observer is based on the Q-filter and the plant model $G(s)$ [27], as shown in Fig. 4(a), where $Q(s)$ is a stable filter, u is the control input, y is the system output, y_r is the reference signal, and $\widehat{d_l}$ is the estimate of the lumped disturbance

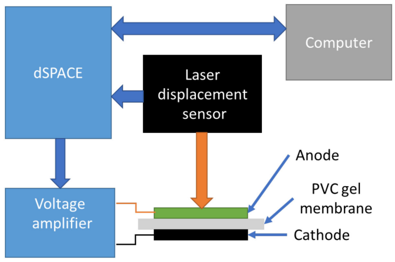

Fig. 5. Experimental setup for the characterization and control of the PVC gel actuator.

TABLE I
THICKNESSES OF PVC GEL ACTUATOR LAYERS

Layer	Material	Thickness	Units
Anode	Stainless steel mesh	1	mm
Membrane	PVC gel	1	mm
Cathode	Stainless steel foil	0.5	mm

d_l. With the approximate cancelation of the nonlinearity, one can represent the system as in Fig. 4(b).

The performance of disturbance estimation is mainly determined by the low-pass filter $Q(s)$. $Q(s)$ needs to be designed such that its relative degree is no less than that of the model $G(s)$ to make sure that the control structure is realizable, i.e., $Q(s)G^{-1}(s)$ should be proper.

V. EXPERIMENTAL RESULTS

A. Experimental Setup

The data for this investigation was collected by actuating a PVC gel actuator, with the voltage as the input and the displacement as the output. Fig. 5 depicts the experimental setup. A PVC gel membrane is sandwiched between a stainless-steel mesh anode and a stainless-steel foil cathode. Table I shows the thickness of each layer. To detect the displacement, a laser displacement sensor (OADM20I6441/S14F, Baumer Electric) is installed above the actuator. The actuator is driven by a high-voltage amplifier (AMJ-2B20, Matsusada Precision). For control signal generation, data collecting, and processing, a dSPACE system is used.

B. Parameter Estimation and Model Validation

First, to identify the actuator model, sinusoidal voltage inputs of three different amplitudes (300, 350, and 400 V) are applied to a PVC gel actuator, along with three different dc biases (400, 450, and 500 V). These input amplitudes and biases are chosen based on physical considerations: The input voltage shall be above zero to preserve the cathode/anode assignment, and less than 1000 V to avoid damage to the PVC gel actuator. Inputs of seven different frequencies, ranging from 0.1 to 10 Hz, are applied for each combination of the aforementioned voltage amplitudes and biases. The specific range of input frequencies is chosen based on the actuation bandwidth—the actuation output beyond 10 Hz is insignificant. We obtain the amplitude and phase of the displacement at the input frequency using the fast Fourier transform, with which we compute the overall system gain and phase-shift for the given input amplitude, bias, and frequency.

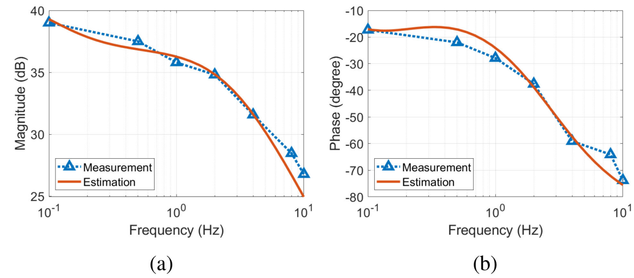

Fig. 6. Measured frequency response of the PVC gel actuator for the amplitude of 300 V and bias of 450 V, and the frequency response of the identified linear model. (a) Magnitude plot. (b) Phase plot.

TABLE II
ESTIMATED POLYNOMIAL PARAMETERS

Polynomial	c_1	c_2	c_3
$n = 1$	1.3664	–	–
$n = 2$	0.1270	1.3057×10^{-5}	–
$n = 3$	0.0721	2.1307×10^{-5}	-1.7231×10^{-11}

The measured (empirical) frequency response (both magnitude and phase responses) for the input with amplitude of 300 V and bias of 450 V is used to identify the LTI component, $G(s)$. As shown in Fig. 6, the empirical response can be captured with a second-order system, identified with the Matlab function *tfest*

$$G(s) = \frac{1.15\ s + 1.03}{s^2 + 17.11s + 8.76} \tag{11}$$

where the units of the input and the output are V and μm, respectively. The function f is identified with different degrees for the polynomial, $n = 1, 2, 3$, and the identified parameters c_i for each case are shown in Table II.

When $n = 1$, the nonlinear function f degenerates into a linear function, resulting in a model that is independent of input amplitude and bias. As seen in Fig. 7, such a model fails to describe input-dependent dynamic behavior. In particular, we note that the measured system gain demonstrates not only clear dependence on the input amplitude, but also dependence on the input bias—for a given input amplitude, the higher the input bias, the higher the system gain. These dependencies, however, are well captured by the proposed nonlinear model, as seen in Figs. 8 and 9, which show the model predictions for the cases of $n = 2$ and $n = 3$, respectively. We note that, if a classical describing function approach were used, one would not be able to account for the observed bias-dependent behavior in the model as the proposed approach does. While it is difficult to tell visually the performance difference between the cases $n = 2$ and $n = 3$, the residual error norm in the least-squares estimation, (10), for the case of $n = 3$ is 23% less than that in the case of $n = 2$.

The dynamic models are further validated with the measured time-domain data from experiments. Fig. 10 shows the comparison of the measured actuator displacement and the model-predicted displacement at two different frequencies for different polynomial degrees ($n = 1, 2, 3$), for input amplitude of 400 V,

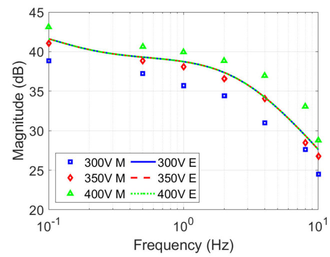

(a)

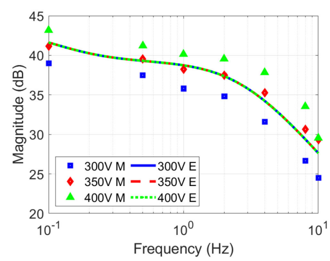

(b)

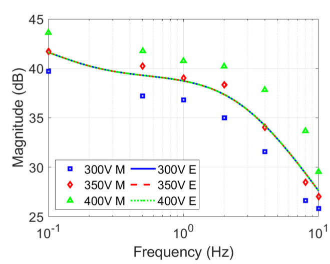

(c)

Fig. 7. Comparison of measured magnitude responses at (a) bias = 400 V, (b) bias = 450 V, and (c) bias = 500 V with model-predicted frequency responses under different input amplitudes $(n = 1)$. The voltages in the legend represent the input amplitude, and "M" and "E" represent the measured data and the model-based estimates, respectively.

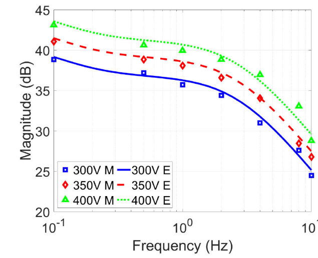

(a)

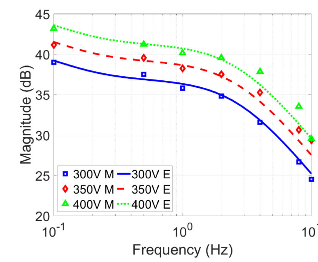

(b)

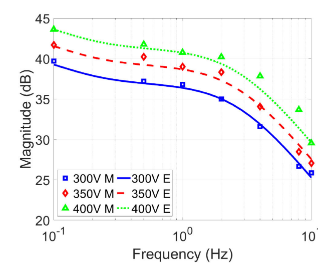

(c)

Fig. 8. Comparison of measured magnitude responses at (a) bias = 400 V, (b) bias = 450 V, and (c) bias = 500 V with model-predicted frequency responses under different input amplitudes $(n = 2)$. The voltages in the legend represent the input amplitude, and "M" and "E" represent the measured data and the model-based estimates, respectively.

and bias of 450 V. These results show that the models with $n = 2$ and $n = 3$ are able to capture well the displacement. With the negligible improvement from $n = 2$ to $n = 3$, it is determined that a model with $n = 2$ would be optimal in striking the trade-off between model accuracy and complexity.

C. Control Experiments

To illustrate the feasibility and effectiveness of the proposed control scheme, several experiments are conducted using the experiment setup shown in Fig. 5. Two types of reference trajectories are used. The first one is a sinusoidal input defined as $y_{r1} = 100 + 25\sin(2\pi f t)\ \mu\text{m}$ and the second one is a multi-harmonic input defined as $y_{r2} = y_{ra} + y_{rb} + y_{rc}$where

$$y_{ra} = 33 + 5\sin(0.2\,\pi\,t)\ \mu\text{m}$$
$$y_{rb} = 33 + 7\sin(\pi\,t)\ \mu\text{m}$$
$$y_{rc} = 30 + 12\sin(2\,\pi\,t)\ \mu\text{m}.$$

For the first-type reference signal, we test it with three different frequencies, 0.1, 0.5, and 1 Hz. Three different control methods are implemented during the experiments, including 1) a classical PID controller, 2) inversion in combination with PID controller (inverse/PID), and 3) inversion in combination with PID controller and disturbance rejection (inverse/PID/DOB). The PID controller is tuned based on the identified $G(s)$ with the PID Tuner app in Matlab, which produces the PID gains given the user-specified trade-offs between performance (i.e., closed-loop bandwidth, or response speed) and robustness (i.e., phase margin) [28]. In this work, we tweaked around the default trade-off levels and tested the different PID gains in experiments until we obtained sound-tracking results under the pure PID control. The same PID gains were then used for the other two controllers (inverse/PID, inverse/PID/DOB). The filter $Q(s)$ is selected as follows:

$$Q(s) = \frac{1}{\lambda s + 1}$$

where $\lambda > 0$. It is known that the smaller λ, the faster transient and lower estimation error for the disturbance observer [29]. However, if λ is chosen too small, $Q(s)G^{-1}(s)$ approaches being improper, which introduces implementation challenges. In this work, $\lambda = 0.1$ is chosen.

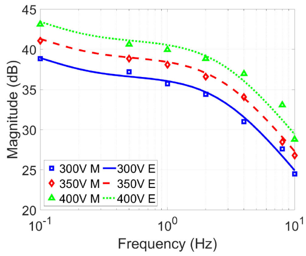

(a)

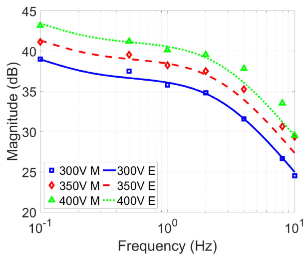

(b)

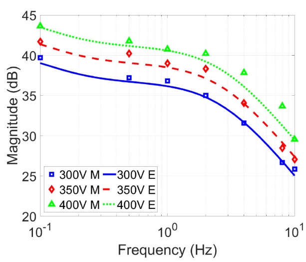

(c)

Fig. 9. Comparison of measured magnitude responses at (a) bias = 400 V, (b) bias = 450 V, and (c) bias = 500 V with model-predicted frequency responses under different input amplitudes ($n = 3$). The voltages in the legend represent the input amplitude, and "M" and "E" represent the measured data and the model-based estimates, respectively.

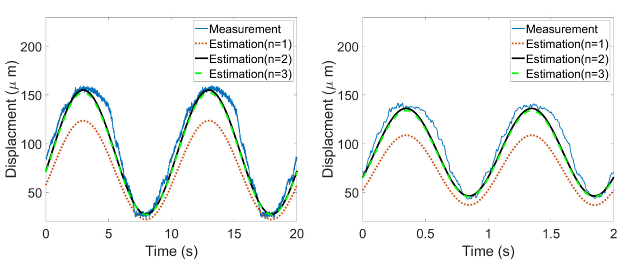

(a) (b)

Fig. 10. Model-predicted output (for $n = 1, 2, 3$) versus measured output for PVC gel actuator with input bias of 450 V and amplitude of 400 V. (a) 0.1 Hz. (b) 1 Hz.

Figs. 11–13 show the comparison between the three controllers (PID, inverse/PID, inverse/PID/DOB) for different reference signals. Table III further summarizes the tracking performance of each control method, including the mean and maximum tracking errors under each reference trajectory. From the results, it can be seen that inverse/PID greatly outperforms the PID controller, and inverse/PID/DOB further improves the tracking accuracy appreciably over inverse/PID. For example, the average tracking error for 1 Hz reference signal is reduced by 63.0% from PID to inverse/PID, and by 83.7% from PID to inverse/PID/DOB.

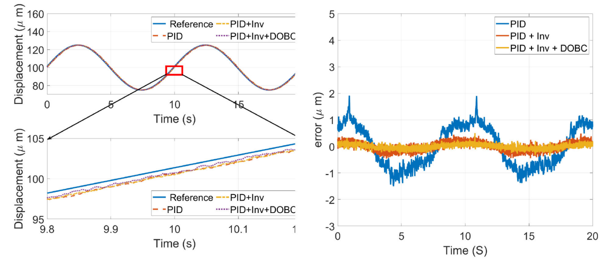

(a) (b)

Fig. 11. (a) Measured displacement versus 0.1 Hz reference under three control schemes (PID, inverse/PID, and inverse/PID/DOB). (b) Comparison of the tracking errors.

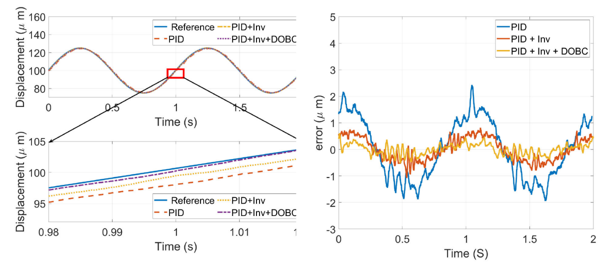

(a) (b)

Fig. 12. (a) Measured displacement versus 1 Hz reference under three control schemes (PID, inverse/PID, and inverse/PID/DOB). (b) Comparison of the tracking errors.

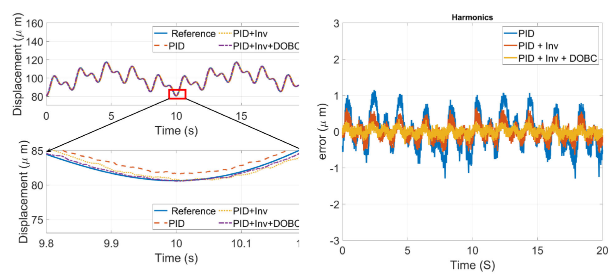

(a) (b)

Fig. 13. (a) Measured displacement versus multiharmonic reference under three control schemes (PID, inverse/PID, and inverse/PID/DOB). (b) Comparison of the tracking errors.

TABLE III
MEAN AND MAXIMUM TRACKING ERRORS UNDER SINUSOIDAL AND MULTIHARMONIC REFERENCE INPUT FOR THREE CONTROLLERS

	PID	Inverse/PID	Inverse/PID/DOB
0.1 Hz (mean)	0.685 μm	0.130 μm	0.072 μm
0.1 Hz (max)	1.914 μm	0.501 μm	0.467 μm
0.5 Hz (mean)	0.968 μm	0.311 μm	0.121 μm
0.5 Hz (max)	2.430 μm	0.753 μm	0.482 μm
1 Hz (mean)	1.024 μm	0.379 μm	0.167 μm
1 Hz (max)	2.552 μm	1.074 μm	0.613 μm
Multi harmonic (mean)	0.394 μm	0.178 μm	0.078 μm
Multi harmonic (max)	1.300 μm	0.666 μm	0.421 μm

VI. Conclusion

In this article, we developed a novel nonlinear dynamic model for PVC gel actuators. The model, which is of Hammerstein-type, consists of a polynomial nonlinearity preceding a linear system. Via a novel extension of the classical describing function method, the developed model was able to predict the experimentally observed dynamic responses under inputs of different amplitudes and biases. We note that an alternative method for parameter identification of the proposed model is to first identify the nonlinearity $f(x)$ with a quasi-static input and then estimate $G(s)$ with the dynamic data for a given choice of input amplitude and bias. The latter approach was not adopted because it is not as amenable to accommodating the varying dynamic behavior at different input amplitudes and biases.

Based on the nonlinear model, a controller was proposed by combining an inverse compensator, a simple PID controller, and a disturbance observer/compensator. The performance of the proposed controller was shown to be superior to a well-tuned PID controller alone, with error reduction by over 80%. While the proposed control framework used the PID as the nominal controller, we note that it could readily accommodate a more advanced nominal controller (e.g., sliding-mode controller or servocompensator), along with the inverse compensator and the disturbance observer/compensator, to deliver potentially even better tracking performance.

For future work, we plan to exploit physical insight into the PVC gel actuation mechanism to develop control-oriented models. In particular, we will leverage our recent study on electric modulus properties of PVC gels [15] to incorporate actuation physics in model development. We will examine the pros and cons of such physical models with respect to the data-driven empirical model presented in this work, including their impact on the control performance. Finally, while this work has focused only on input-dependent nonlinear dynamics, PVC gel actuators also exhibit mild hysteresis behavior. We will improve the dynamic models to capture the hysteresis nonlinearity, and subsequently develop control methods that address both input-dependent nonlinear dynamics and hysteresis.

References

[1] H. R. Choi *et al.*, “Biomimetic soft actuator: Design, modeling, control, and applications,” *IEEE/ASME Trans. Mechatronics*, vol. 10, no. 5, pp. 581–593, Oct. 2005.

[2] M. A. Sharif, H. Lei, M. K. Al-Rubaiai, and X. Tan, “Ionic polymer-metal composite torsional sensor: Physics-based modeling and experimental validation,” *Smart Mater. Struct.*, vol. 27, 2018, no. 7, Art. no. 075039.

[3] Y. Li and M. Hashimoto, “Design and prototyping of a novel lightweight walking assist wear using PVC gel soft actuators,” *Sensors Actuators A: Phys.*, vol. 239, pp. 26–44, 2016.

[4] Y. Li, Y. Li, and M. Hashimoto, “Low-voltage planar PVC gel actuator with high performances,” *Sensors Actuators B: Chem.*, vol. 282, pp. 482–489, 2019.

[5] T. Hwang, Z. Frank, J. Neubauer, and K. J. Kim, “High-performance polyvinyl chloride gel artificial muscle actuator with graphene oxide and plasticizer,” *Sci. Rep.*, vol. 9, no. 1, pp. 1–9, 2019.

[6] A. Furuse and M. Hashimoto, “Development of novel textile and yarn actuators using plasticized PVC gel,” in *Proc. Electroactive Polym. Actuators Dev.*, 2017, Art. no. 1016327.

[7] Y. Li, M. Guo, and Y. Li, “Recent advances in plasticized PVC gels for soft actuators and devices: A review,” *J. Mater. Chem. C*, vol. 7, no. 42, pp. 12991–13009, 2019.

[8] M. Ali, T. Ueki, D. Tsurumi, and T. Hirai, “Influence of plasticizer content on the transition of electromechanical behavior of PVC gel actuator,” *Langmuir*, vol. 27, no. 12, pp. 7902–7908, 2011.

[9] T. Hirai, T. Ogiwara, K. Fujii, T. Ueki, K. Kinoshita, and M. Takasaki, “Electrically active artificial pupil showing amoeba-like pseudopodial deformation,” *Adv. Mater.*, vol. 21, no. 28, pp. 2886–2888, 2009.

[10] Y. Li, Y. Maeda, and M. Hashimoto, “Lightweight, soft variable stiffness gel spats for walking assistance,” *Int. J. Adv. Robotic Syst.*, vol. 12, no. 12, 2015, Art. no. 175.

[11] W.-H. Park, E.-J. Shin, Y. Yoo, S. Choi, and S.-Y. Kim, “Soft haptic actuator based on knitted PVC gel fabric,” *IEEE Trans. Ind. Electron.*, vol. 67, no. 1, pp. 677–685, Jan. 2020.

[12] W.-H. Park, E.-J. Shin, and S.-Y. Kim, “Enhanced design of a soft thin-film vibrotactile actuator based on PVC gel,” *Appl. Sci.*, vol. 7, no. 10, 2017, Art. no. 972.

[13] T. Hirai *et al.*, “Characteristic electrical actuation of plasticized poly(vinyl chloride): Various electrical functions in relation with the dielectric plasticizers,” in *Proc. Adv. Sci. Technol.*, 2013, pp. 1–6.

[14] Z. Wang, Y. Wang, Z. Wang, Q. He, C. Li, and S. Cai, “3D printing of electrically responsive PVC gel actuators,” *ACS Appl. Mater. Interfaces*, vol. 13, no. 20, pp. 24164–24172, 2021.

[15] H. Xia and T. Hirai, “Space charge distribution and mechanical properties in plasticized PVC actuators,” in *Proc. Int. Conf. Mechatronics Automat.*, 2009, pp. 164–169.

[16] Z. Frank, M. Al-Rubaiai, X. Tan, and K. J. Kim, “A study of electroactive polyvinyl chloride (PVC) gel actuators through the use of the electric modulus formalism and cyclic linear voltage sweeps,” *Smart Mater. Struct.*, vol. 31, no. 3, 2022, Art. no. 035020.

[17] K. Asaka and M. Hashimoto, “Electrical properties and electromechanical modeling of plasticized PVC gel actuators,” *Sensors Actuators B: Chem.*, vol. 273, pp. 1246–1256, 2018.

[18] M. Shibagaki, N. Ogawa, and M. Hashimoto, “Modeling of a contraction type PVC gel actuator,” in *Proc. IEEE Int. Conf. Robot. Biomimetics*, 2010, pp. 1434–1439.

[19] Y. Li and M. Hashimoto, “PVC gel based artificial muscles: Characterizations and actuation modular constructions,” *Sensors Actuators A: Phys.*, vol. 233, pp. 246–258, 2015.

[20] K. Asaka and M. Hashimoto, “Electromechanical modeling of plasticized PVC gel actuators and the improvement in their performances with the additions of ionic liquids,” in *Proc. Electroactive Polym. Actuators Devices XXII*, 2020, Art. no. 1137511.

[21] Z. Frank, Z. Olsen, T. Hwang, and K. J. Kim, “Modelling and experimental study for PVC gel actuators,” in *Proc. Dyn. Syst. Control Conf.*, 2019, Art. no. V003T20A007.

[22] M. Hashimoto, “Development of an artificial muscle using PVC gel,” in *Proc. ASME Int. Mech. Eng. Congr. Expo.*, 2011, pp. 745–754.

[23] D. Chowdhury, Y. K. Al-Nadawi, and X. Tan, “Dynamic inversion-based hysteresis compensation using extended high-gain observer,” *Automatica*, vol. 135, 2022, Art. no. 109977.

[24] M. Al-Rubaiai *et al.*, “Control-oriented nonlinear modeling of polyvinyl chloride (PVC) gel actuators,” *IFAC-PapersOnLine*, vol. 54, no. 20, pp. 304–309, 2021.

[25] J.-J. E. Slotine and W. Li, *Applied Nonlinear Control*, vol. 199. Englewood Cliffs, NJ, USA: Prentice-Hall, 1991.

[26] R. T. Seeley, *An Introduction to Fourier Series and Integrals*. Mineola, NY, USA: Courier Corporation, 2014.

[27] W.-H. Chen, J. Yang, L. Guo, and S. Li, “Disturbance-observer-based control and related methods—An overview,” *IEEE Trans. Ind. Electron.*, vol. 63, no. 2, pp. 1083–1095, Feb. 2016.

[28] “PID tuning algorithm,” 2022. [Online]. Available: https://www.mathworks.com/help/control/getstart/pid-tuning-algorithm.html

[29] S. Li, J. Yang, W.-H. Chen, and X. Chen, *Disturbance Observer-Based Control: Methods and Applications*. Boca Raton, FL, USA: CRC Press, 2014.